Ocular dominance patterns and the wire length minimization: a numerical study

Alexei A. Koulakov and Dmitri B. Chklovskii

Cold Spring Harbor Laboratory, Cold Spring Harbor, NY 11724

(Dated: April 8, 2002)

We study a mathematical model for ocular dominance patterns (ODPs) in primary visual cortex. This model is based on the premise that ODP is an adaptation to minimize the length of intracortical wiring. Thus we attempt to understand the existing ODPs by solving a wire length minimization problem. We divide all the neurons into two classes: left- and right-eye dominated. We find that segregation of neurons into monocular regions reduces wire length if the number of connections to the neurons of the same class (intraocular) differs from the number of interocular connections. The shape of the regions depends on the relative fraction of neurons in the two classes. We find that if both classes are almost equally represented, the optimal ODP consists of interdigitating stripes. If one class is less numerous than the other, the optimal ODP consists of patches of the less abundant class surrounded by the neurons of the other class. We predict that the transition from stripes to patches occurs when the fraction of neurons dominated by the underrepresented eye is about 40%. This prediction agrees with the data in macaque and Cebus monkeys. We also study the dependence of the periodicity of ODP on the parameters of our model.

PACS numbers:

I. INTRODUCTION

In the primary visual area (V1) of many mammals, most neurons respond to the stimulation of two eyes unevenly: they are either right or left eye dominated. In some species, right/left eye dominated neurons are segregated and form a system of alternating monocular regions known as the ocular dominance pattern (ODP) (Wiesel and Hubel, 1965, 1969). In others, ODP is not observed (see Horton and Hocking, 1996b for a comprehensive list of species). ODPs, when observed, vary significantly between different species and even between different parts of V1 in the same animal.

Most modeling studies of ODP (Erwin et al., 1995; Swindale, 1996) have addressed its development. They succeeded in generating ODPs of realistic appearance. However, several *why* rather than *how* questions remained unanswered. For instance, (1) why, from functional point of view, do the ODPs exist? (2) Why do some mammalian species exhibit ODPs while others do not (Horton and Hocking, 1996b; Livingstone, 1996)? (3) Why do the monocular regions have different appearance (stripes as opposed to patches) between different parts of V1 within the same animal (LeVay et al., 1985)?

The question of functional significance of ODPs has been addressed theoretically using the wiring economy principle (Mitchison, 1991; Chklovskii, 2000). The idea is that evolutionary pressure to keep the brain volume to a minimum requires making the wiring (axons and dendrites) as short as possible, while maintaining neuronal functional properties (Cajal, 1995; Allman and Kaas, 1974; Cowey, 1979; Cherniak, 1992; Young, 1992; Chklovskii et al., 2001; Koulakov and Chklovskii, 2001). In many cases these functional properties are specified by the rules of establishing connections between neurons, or wiring rules. The problem presented by the wiring economy principle is therefore to find, for given wiring rules, the spatial neuronal layout that minimizes the total connection length. This approach allows to understand many features in cortical maps, such as orientation preference maps (Koulakov and Chklovskii, 2001), as evolutionary adaptations, which minimize the total cortical volume.

The goal of this study is to find the simplest model, which on one hand is supported by experimental evidence, and on the other encompasses most of OD phenomenology. The use of the simple model allows us to explore its parameter space completely and to give answers to the set of questions above. We also evaluate the dependence of the ODP period on the parameters of our model and compare it to the ODP periodicity observed in macaque monkey. We find that the experimentally observed variation of the period is in agreement with the wiring economy theory.

II. MODEL AND METHODS

A. Description of the model

For the purposes of minimizing the cortical wiring we consider only intra-cortical connections since they constitute the majority of gray matter wiring (LeVay and Gilbert, 1976; Peters and Payne, 1993; Ahmed et al., 1994). We therefore disregard the thalamic afferents and other extra-cortical projections. In an attempt to make wiring economy argument more quantitative, we propose a model describing the component of intracortical cir-

cuitry sensitive to OD. The principal elements of our model are therefore the connection rules between cortical neurons. To assess the sensitivity of the intracortical wiring to OD we examine the connections in the cortical layer $4C\beta$, where OD is most strongly pronounced. Such sensitivity has been studied by Katz et al. (1989). They made three observations regarding the wiring rules:

i) Neurons in the layer $4C\beta$ near the interface between two OD columns arborize more in home rather than in the opposite eye column. Therefore neurons establish more connections with the neurons dominated by the same rather than by the opposite eye.

ii) Axons and dendrites of these neurons have a tendency to bend away from the interface between OD columns. This implies that not only they avoid penetration to the opposite OD column but also they attempt to maintain sufficiently high number of connections in the home column.

iii) Axons or dendrites penetrating through the opposite eye column to the next same eye column are *never* observed. This means that retinotopy has little effect on connections in layer $4C\beta$. Indeed the neurons on the edges of two same eye columns separated by one opposite eye column have on average receptive fields centered next to each other. If connections in $4C\beta$ were sensitive to the retinotopic coordinates, these two edges should be connected (Mitchison, 1991). However out of 21 cells examined Katz et al. (1989) observed *none* producing axons reaching the next same eye domain. The only possibility for such cells to be connected is due to the overlap between dendritic and axonic arbors of two cells separated by more than 500 μm. Such possibility is small because of the strong repulsion of the connections by the opposite eye column located between two cells (observation *i)*).

These three observations lay the basis of our model which we now describe. The elementary unit of our model mimics the columnar organization of the cortex (Mountcastle, 1957) and uniformity of ODP along the direction normal to the slab. The elementary unit is therefore a microcolumn, which is defined as a box, spanning the cortex perpendicular to its surface, whose other two dimensions are smaller than the characteristic scale of ODP ($\approx 500\mu$), and yet large enough to include many neurons. A possible choice of dimensions for such a microcolumn is *thickness of cortex* ($\approx$ 1.5mm) $\times\, 30\mu \times 30\mu$, in which case it includes about 310 cells in V1 (Rockel et al., 1980). The microcolumn units are therefore arranged on a square lattice with 30μ period.

Although the choice of the elementary unit size may seem arbitrary, the results of our calculation are independent of the choice. The size of the unit is analogous to the integration step, which does not affect the value of an integral significantly if chosen to be small enough.

Motivated by the second observation in layer $4C\beta$ listed above, i.e. that neurons maintain a fixed number of connections in the home OD column, we make the following assumption about the connection rules. Each microcolumn unit must establish connections with N_s distinct units dominated by the same eye and N_o units dominated by the opposite eye. These connection rules are illustrated in Fig. 1.

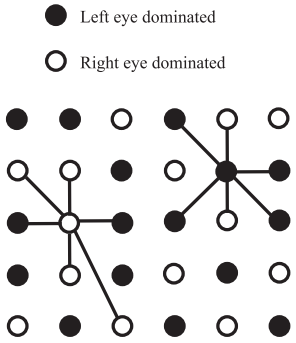

FIG. 1 Our model illustrated. The units dominated by the left and right eyes are shown by the full and empty circles respectively. Each unit is *required* to make N_s connections to the units of the same OD and N_o connections to the units of the opposite OD. In this illustration $N_s = 4$ and $N_o = 2$. The connections satisfying these rules are shown for two units, right and left eye dominated. Small numbers of connections are chosen for the ease of illustration; in actual implementation of the model both N_s and N_o are large (see below).

Only the relative values of N_s and N_o (rather than absolute) are important because of the arbitrariness in the definition of microcolumn. Thus, if a $30 \times 30\mu$ microcolumn receives $N_s = 10^4$ projections from the same OD column and $N_o = 10^3$ projections from the opposite OD column, a $60 \times 60\mu$ microcolumn receives four times less projections respectively, or $N_s = 2.5 \cdot 10^3$ and $N_o = 2.5 \cdot 10^2$. This is because with coarser units each projection is more effective: connecting to one $60 \times 60\mu$ unit implies connecting to four $30 \times 30\mu$ units. Both these implementations of the model produce the same OD pattern, discretized in "pixels" of different size. The important quantity, which is invariant with respect to the change of "pixel"/microcolumn size, is the ratio between N_s and N_o (equal to 10 in this example). This is the first parameter of our model.

The second parameter of our model is the filling fraction of the units (microcolumns) dominated by the left eye afferents f_L with respect to the total number of units, averaged over several ODP periods. This parameter is the fraction of the left eye dominated units f_L by $f_L + f_R = 1$. For the majority of important cases $f_L = f_R = 1/2$, however on the periphery of visual field one of the eyes (ipsilateral) is underrepresented. Therefore, its filling fraction is less than 1/2.

The third observation above implies that the component of connections sensitive to OD is not sensitive to the retinotopy, and both numbers N_s and N_o do not depend on the position of the receptive field of the unit. This may be due to significant scatter of the receptive field of the cells within cortical column on the scales of about 1mm (Hubel and Wiesel, 1974). The position of the receptive

field of the microcolumn is therefore vaguely defined and cannot affect OD sensitive connections significantly.

B. Methods

Given these wiring rules we look for an optimal layout of the microcolumn units which minimizes the total length of connections. To find the layout minimizing the total wirelength we employ a combination of computational and analytical techniques. To make our choice of methods clear we first comment on the expected properties of the solution.

A possible solution of our model is the *Salt and Pepper* layout in which the units dominated by right and left eyes are uniformly intermixed. In this layout the units belonging to different eyes are not segregated, ODP is not formed, and the local values of the filling fraction are equal to 1/2 (by local value we understand an average over a domain including many units yet small compared to the period of ODP). It should be contrasted to the case when units dominated by the same eye fill in large domains i.e. form the ODP. In the latter case the local values of the filling factor of each eye vary from 0 to 1. However one can imagine an intermediate situation when the local filling fraction varies from $1/2 - a$ to $1/2 + a$, where the amplitude of variation $0 < a \ll 1/2$. This corresponds to the case of *weak segregation* into ODP. The weak segregation is found in squirrel monkey where ODP has fuzzy appearance and until recently was suspected not to be formed (Horton and Hocking, 1996). If $a = 1/2$, i.e. the local filling fraction varies from 0 to 1, the ODP's have sharp appearance. Using the general terminology from binary mixtures (cite diblock copolimer paper) we call this regime the *strong segregation* limit.

The methods useful in the strong segregation limit are not good in the weak segregation case and vice versa. We use the simulated annealing to find the optimum phases for the strong and nearly strong segregation cases. Having found the optimum phase in the strong segregation case to assess the period of ODP we use the exact enumeration technique, which compares layouts belonging to the same phase with different periods. The treatment of the weak segregation case requires the use of continuous variables and is done employing the perturbation theory. Below we describe these methods in more detail.

1. Simulated annealing

The parameters of Metropolis Monte-Carlo method (Metropolis et al., 1953) are optimized to render most consistent results for multiple restarts. We use square 20×20 array of units with periodic boundary conditions. The units are either left or right eye dominated. At each step the algorithm attempts to change the dominance of one unit to the opposite. The value of the average filling fraction f_{L0} is enforced by adding the following term to the total connection length:

$$\delta L = 20.0 L \frac{(f_L - f_{L0})^2}{1/f_{L0} + 1/(1 - f_{L0})}, \qquad (1)$$

where L and f_L are the current values of the total wirelength and average filling fraction. Such term in the functional keeps the current value f_L close to the required value f_{L0}.

To map out the phase diagram the values of f_L change from 0.2 to 0.8 in 0.02 increments. The values of N_s and N_o satisfy the condition $N_s + N_o = 30$ and are changed in unit increments, i.e. have the following values: 12, 18; 13, 17; 14, 16; 15, 15; 16, 14; etc. The phases at the intermediate points are taken from the nearest points, where result is available.

The Monte-Carlo temperature is gradually annealed from $0.24L/N$ to $0.008L/N$ ($N = 400$ is the total number of units) in 5000 sweeps through the entire system ($20 \times 20 \times 5000$ steps). The resulting layout is then examined and the phases visually identified.

2. Perturbation theory

Salt and Pepper layout is relatively easy to study due to its uniformity, and can be solved exactly (Chklovskii and Koulakov, 2000). If a layout does not deviate significantly from *Salt and Pepper*, i.e. the weak segregation case takes place, it can also be solved exactly. This implies that the wire length can be written as an explicit functional of density distribution of the units. Such functional was evaluated and optimized with respect to the density variations by Chklovskii and Koulakov (2000). The optimization shows that ODPs are formed for the values of parameter $|N_s - N_o|/N_s > 0.02$. However the simulated annealing method cannot distinguish weak segregated ODP from *Salt and Pepper* for $|N_s - N_o|/N_s < 0.2$. There are two reasons for the failure of simulated annealing to do so:

- Simulated annealing is performed at small but finite temperature that destroys weakly segregated ODP.

- The units can be either completely right or left eye dominated. This implies that OD can change only sharply in the described annealing version. This is useful for obtaining the strongly segregated phases, which occupy major part of the parameter space. However, in the weak segregation limit the local OD changes smoothly. Thus used version of simulated annealing performs poorly at $N_s \approx N_o$.

We therefore replace the simulated annealing results by those from Chklovskii and Koulakov (2000) at small values of parameter $N_s - N_o$ (see the phase diagram below).

3. Calculation of the ODP period.

To evaluate the period of ODP precisely, we first determine the phase (*Salt and Pepper*, *Stripes*, or *Patches*) for the given set of parameters N_s/N_o and f_L, using methods described above. We then take a lattice containing a large number of units, which exceeds sufficiently the lattice used in simulated annealing. This is possible because the method of determining period described below is much less time consuming than simulated annealing. We then arrange the two types of units on the lattice, using ODP determined by the simulated annealing, and vary the period of the pattern to find the period producing the minimum of the wire length. Below we describe the procedure for both *Stripes* and *Patches* in more details.

i) Stripes

To find the optimum period for stripes we use an array containing 300 by 300 units. This array includes three periods of the stripes, which run parallel to one of the sides of the region. Each period therefore includes 100 units, containing n_L left and n_R right eye units, $n_L+n_R=100$. By varying n_L we accomplish the change in the filling fraction of the left (ipsilateral) eye, according to the formula: $f_L = n_L/(n_L+n_R)$. We consider a string of 100 units at the center of the array, which is representative of all the units in the configuration. For each of the central units the computer program establishes connections, according to the connection rules. Most of the calculations are done for $N_s+N_o=300$. We check that results change for different N_s+N_o in a predictable fashion (see below, Results, subsection III.D.1). Stripes therefore have a fixed period in terms of number of units (100). To find the optimal spatial period of the stripes we vary the shape of each elementary cell in the 300 by 300 array. Thus, if the rectangular cell dimensions are a_x perpendicular and a_y parallel to the stripes, we vary both a_x and a_y, keeping the area of elementary cell $a_x a_y = 1$ constant. By doing so we do not change the density of units, but vary the spatial OD period, according to the formula $\Lambda = 100 a_x$. For each value of a_x the cells are reconnected according to the connection rules. Special care is taken about exclusion of the boundary effects by making sure that none of the units on the edges of the array is connected to. After the optimum period is found the period in terms of number of units is changed from 100 to another value, closer to the value of spatial period, to check for the absence of geometric artifacts, associated with distortions of elementary cells. The change of the spatial period after this procedure is typically absent but in extreme cases does not exceed 3%.

ii) Patches

Since our results indicate that a triangular crystal of *Patches* is formed (see Fig. 7J), we consider an array in the shape of parallelogram commensurate with the triangular arrangement of *Patches*. The lattice sites in the array, representing units, are also arranged on a triangular lattice. Their positions are given by $x(i,j) = i + j/2$ and $y(i,j) = j\sqrt{3}/2$, where i and j are integers varying between 1 and $5l$. Here l is the period of ODP to be optimized. The centers of *Patches* are located at points $x_c n, m = ln + lm/2$ and $y_c(n,m) = lm\sqrt{3}/2$. Each patch includes lattice sites at the distance from a center determined by the filling fraction of the ipsilateral eye: $R = l\sqrt{f_L\sqrt{3}/2\pi}$. The units within/outside the patch are left/right eye dominated. The units in the configuration are then represented by the central parallelogram: $i, j = (2l+1)..3l$. For each of the units connections are made according to the connection rules with $N_s + N_o = 300$. The optimum period is obtained by varying parameter l.

4. Fourier analysis of the ocular dominance patterns

To determine the experimental dependence of the ODP period on the filling factor, the image of ODP in macaque monkey (Horton and Hocking, 1996a) is converted into a digital format. In this format the image is represented by a set of pixels. A pixel with coordinates x and y is represented by a number $s(x,y)$, equal to 0 for the right eye dominated and 1 for the left eye dominated area. For each position in the image we then determine the local value of the average filling fraction of the ipsilateral eye and the value of local OD period. Both these calculations are similar. To do the calculation at a certain point in the map, given by coordinates (x_0, y_0), we surround the corresponding pixel by a square, containing 64×64 pixels (black square in Fig. 2, 3.7×3.7mm). The dimensions of the square are such that one hand it contains a few ODP periods (about 3), which is needed for averaging, and on the other hand it is small compared to the characteristic dimensions over which the properties of ODP change ($\sim$ 1cm, see Fig. 2). To determine the filling fraction we average the scanned image over the square: for position (x_0, y_0) in the map the local value of the average filling fraction is given by

$$f_L(x_0,y_0) = \frac{1}{64\times64}\sum_{x=x_0-31}^{x_0+32}\sum_{y=y_0-31}^{y_0+32} s(x,y). \qquad (2)$$

To determine the local value of ODP period we perform the Fourier transform of the $s(x,y)-f_L$ in the square. As a result we obtain a set of numbers $\tilde{s}(q_x,q_y)$, representing the Fourier transform amplitudes, defined on a 64×64 set of wave vectors (q_x,q_y). The spectral power, represented by $|\tilde{s}(q_x,q_y)|^2$, is shown in Fig. 3 for one of the points in the pattern, corresponding to *Stripes*. It clearly has a bimodal appearance, indicating the average in the square direction of the stripes. We then determine the average value of the wave vector, using the formula:

$$\langle q(x_0,y_0)\rangle = \frac{\sum_{q_x,q_y}\sqrt{q_x^2+q_y^2}\,|\tilde{s}(q_x,q_y)|^2}{\sum_{q_x,q_y}|\tilde{s}(q_x,q_y)|^2}. \qquad (3)$$

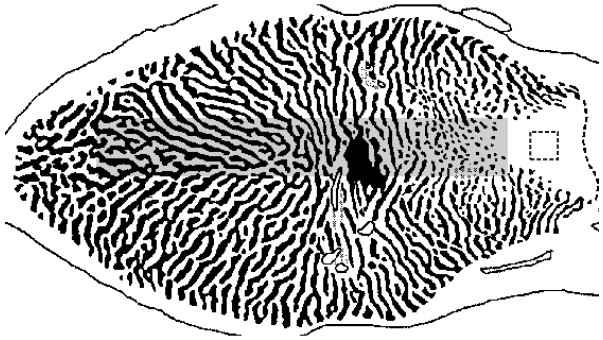

FIG. 2 The image of the striate cortex of macaque monkey 1 left hemisphere from Horton and Hocking (1996a). The left/right eye dominated areas are shown by black/white. For the pixels in the shaded area we evaluate the filling factor and OD period, displayed in Fig. 17 below. The dashed square gives an example of the region containing 64 by 64 pixels, for which the filling fraction and Fourier transform are calculated. It has dimensions 3.7 by 3.7 mm.

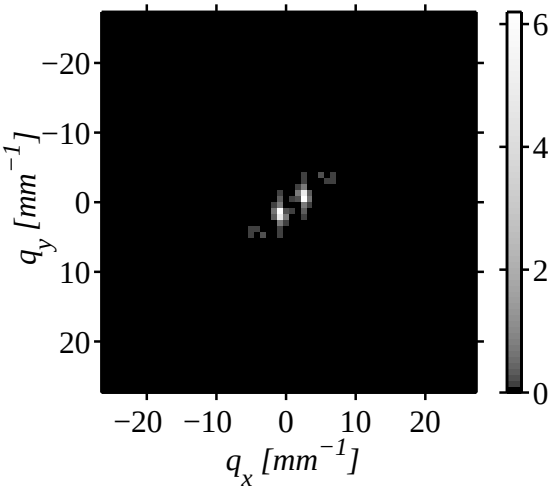

FIG. 3 The spectral power for a point in the pattern occupied by stripes. The spectrum has the bimodal appearance, characteristic of stripes. The direction of the modes is determined by the direction in which ODP changes (perpendicular to stripes). The distance of the modes from the center determines the local value of ODP period by Eq.(4). The spectral power in the scale bar is in arbitrary units.

The value of the mean ODP period is then defined as

$$\Lambda\left(x_0, y_0\right) = \frac{2\pi}{\left\langle q\left(x_0, y_0\right)\right\rangle}. \tag{4}$$

This value for each pixel in the shaded area in Fig. 2 is shown in Fig. 17.

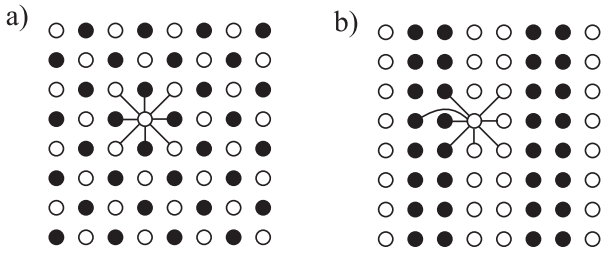

FIG. 4 Ocular dominance patterns for $f_L = 1/2$ and $N_s = N_o = 4$. (a) A realization of the *Salt and Pepper* phase gives minimal wire length ($l \approx 9.67$ lattice constants per neuron). (b) A realization of the *Stripe* phase is suboptimal ($l \approx 10.24$).

III. RESULTS

A. Small number of connections

We start by finding optimal layouts for three illustrative examples of wiring rules with small numbers of connections, N_s and N_o. We caution the reader that because of the small numbers of connections phase assignments may seem arbitrary. These examples are chosen to illustrate our main results which will be confirmed both in the lattice model with large N_s and N_o later in this section and in the continuous model (Chklovskii and Koulakov, 2001).

For the first two examples we set equal numbers of left and right dominated neurons, $f_L = f_R = 1/2$. In the first example each neuron connects with equal numbers of the same-eye and other-eye neurons, $N_s = N_o = 4$. Then the optimal layout is the "chess board" of left/right neurons, Fig.4a. This layout is a realization of the *Salt and Pepper* phase, Fig.7a, because each neuron has an equal number of left and right neurons among its immediate neighbors. To calculate the length of connections per neuron, l, we notice that in this layout all neurons have the same pattern of connections. By considering one of them, Fig.4a, we find that $l = 4 + 4\sqrt{2} \approx 9.67$. This layout is optimal because each neuron makes all of its connections with immediate neighbors.

A suboptimal layout for the same wiring rules is illustrated by a realization of the *Stripe* phase, Fig.4b. In this layout each neuron has the same pattern of connections up to a mirror reflection. By considering one of them, Fig.4b, we find $l = 6 + 3\sqrt{2} \approx 10.24$, greater than $l \approx 9.67$ for the *Salt and Pepper* phase. Here each neuron has among its immediate neighbors only three other-eye neurons, while the wiring rules require connecting with four other-eye neurons. A connection to a more distant neighbor is longer making the layout suboptimal. We confirm the optimality of the *Salt and Pepper* phase for $N_s = N_o$ for large N_s, N_o both numerically and analytically.

In the second example each neuron connects with more same-eye than other-eye neurons: $N_s = 5$, $N_o = 3$. Then a realization of the *Salt and Pepper* phase, Fig.5a is not

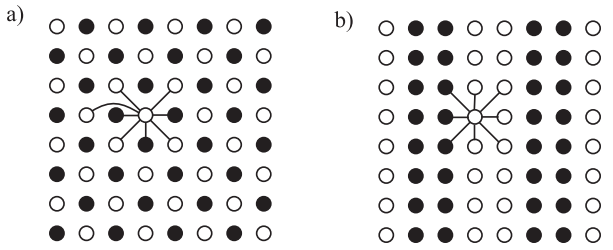

FIG. 5 Ocular dominance patterns for $f_L = 1/2$ and $N_s = 5$, $N_o = 3$. (a) A realization of the *Salt and Pepper* is suboptimal ($l \approx 10.24$). (b) A realization of the *Stripe* phase gives minimal wire length ($l \approx 9.67$).

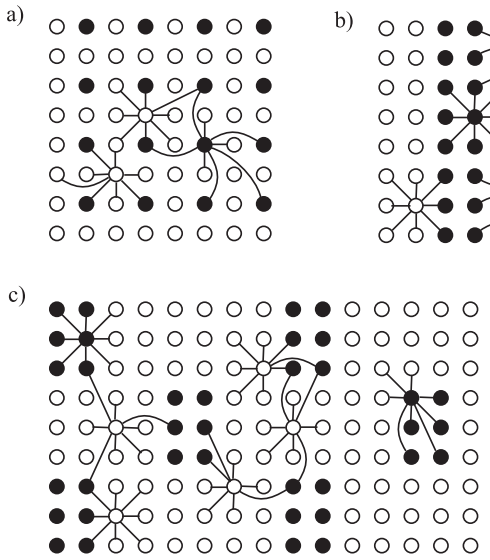

FIG. 6 Ocular dominance patterns for $f_L = 1/4$ and $N_s = 5$, $N_o = 3$. Realizations of the (a) *Salt and Pepper* ($l \approx 11.26$) and (b) *Stripes* ($l \approx 11.49$) are suboptimal. (c) A realization of the *L-Patch* phase gives minimal wire length ($l \approx 10.67$).

optimal anymore. The length of connections per neuron is $l \approx 10.24$, while the *Stripe* phase, Fig.5b gives $l \approx 9.67$. The *Salt and Pepper* phase loses in wiring efficiency because there are not enough same-eye neurons among immediate neighbors and connections with more distant neighbors are needed. The *Stripe* phase, Fig.5b rectifies this inefficiency by having each neuron make connections only with immediate neighbors. Thus, clustering of same-eye neurons is advantageous if each neuron connects more with the same-eye than with the other-eye neurons.

In the third example we use the same wiring rules ($N_s = 5$, $N_o = 3$) but take different numbers of left/right neurons, $f_L = 1/4$, $f_R = 3/4$. The realizations of the *Salt and Pepper* phase is shown in Fig.6a and of the *Stripe* phase in Fig.6b. In these layouts, different neurons have different patterns of connections. To find the wiring length per neuron we average over different patterns and find for the *Salt and Pepper* phase $l \approx 11.26$ and for the *Stripe* phase $l \approx 11.49$. A more efficient layout is the *L-Patch* phase, Fig.6c, where $l \approx 10.67$. Although we cannot prove that the *L-Patch* phase is optimal, this seems likely. Thus, the optimal shape of monocular regions depends on the relative numbers of left/right neurons.

B. The shape of OD columns

After giving some examples of ODPs with small numbers of connections N_s and N_o we discuss the opposite case of large numbers. As we show below in Section III.D.1, the shape of OD columns in this case does not depend on the absolute values of parameters N_s and N_o. It is determined by the ratio N_s/N_o and by the relative amount of ipsilateral neurons f_L (assuming that the left eye is ipsilateral). Depending on the values of parameters N_s/N_o, and f_L, optimal layout belongs to the one of the eight phases shown in Fig. 7, where ipsilateral and contralateral-eye dominated neurons are shown by black and white regions respectively. These phases can be divided into three major classes. The first class is represented by the unsegregated *Salt and Pepper* layout, in which two types of neurons are uniformly intermixed (Figure 7A). The second class includes *Stripy* layouts, shown in Figures 7C, E, G, I. The third class consists of *Patchy* layouts, displayed in Figures 7D, F, H, G.

We distinguish several subclasses of *Stripy* phases. First, it is the sharp *Stripes* (Figure 7I), which consists of alternating lamellar monocular regions. Second, it is the weakly segregated *Stripes* (Figure 7C,E). In this ODP the variation of density of left/right eye dominated neurons is small. This is an intermediate pattern between the unsegregated *Salt an Pepper* and the sharp *Stripe* layouts. This phase is therefore fragile and difficult to obtain numerically. In some cases simulated annealing can produce such a phase, Figure 7E. In the other cases the weak segregated phase can only be obtained by the perturbation theory, which can carefully account for a weak variation of neuronal density. Such case is shown in Figure 7C. Third, we also obtain *Stripy* phases that show a tendency to become *Patches*, by e.g. their longitudinal modulation, such as shown in Figure 7G.

Similar subclasses exist among *Patchy* layouts. We obtain sharp, weakly segregated (obtained from simulated annealing or perturbation theory), and elongated *Patches*, which are shown in Figures 7J, F, D, and H respectively. Finally, there are mixed phases containing both *Stripes* and *Patches*, such as in Figure 7B. These ODP's are shown on the phase diagram (PD) in Figure 8. The phase diagram shows the optimum phase (minimizing the total wire length) for given values of parameters N_s/N_o and f_L.

The important feature of the PD is its left-right eye symmetry. It is apparent from the symmetry of Figure 8 with respect to the line $f_L = 1/2$. This is a consequence of the left-right eye symmetry of our model, implying that the connection rules, defined by numbers N_s and N_o are independent on whether a neuron is left or right-

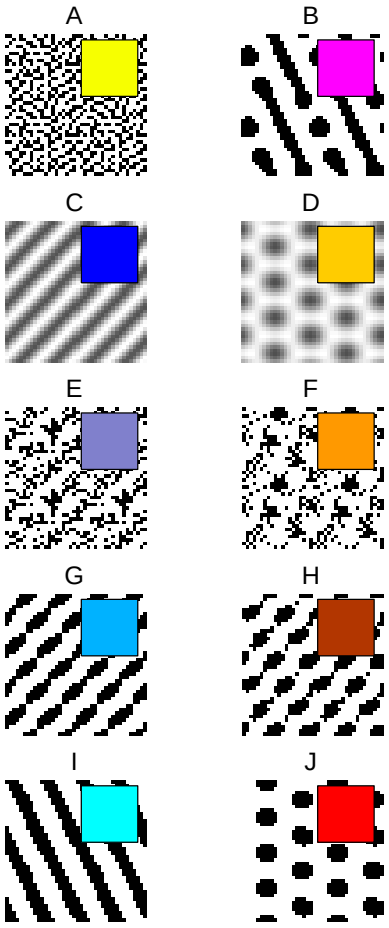

FIG. 7 The phases obtained by perturbation theory (**C** and **D**) and by simulated annealing (the rest). Each simulation array of 20 by 20 units in reproduced 4 times in each Figure. The color bar is the key for Figure 8. **A**: *Salt and Pepper*; **B**: *Stripes* mixed with *Patches*; **C** and **D**: weakly segregated *Stripes* and *Patches* obtained by the perturbation theory; **E** and **F**: weakly segregated *Stripes* and *Patches* obtained by simulated annealing; **G**: modulated *Stripes*; **H**: elongated *Patches*; **I**: sharp *Stripes*; **J**: sharp *Patches*;

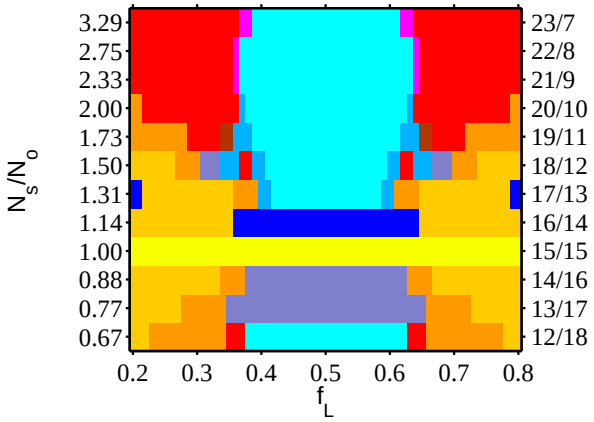

FIG. 8 The phase diagram showing the optimum phase for given values of parameters f_L and N_s/N_o. For the color key see Figure 7.

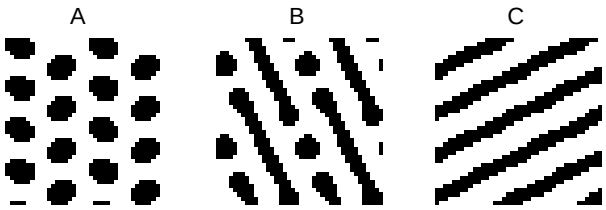

FIG. 9 The example of transition from *Patches* to *Stripes* at $N_s/N_o = 3$. **A**, **B**, and **C** show the optimum phases for $f_L = 0.34$, 0.36, and 0.38 respectively.

eye dominated. For this reason the phase for $f_L > 1/2$ can be obtained from the point with the same N_s/N_o and the value of the filling fraction equal to $1 - f_L < 1/2$. This corresponds to the replacement of the white regions in Figure 7 by black and vice versa. A similar correspondence takes place when one compares ODP's in left and right hemisphere.

Another important feature of the PD is the existence of the *Salt and Pepper* region around the line $N_s/N_o = 1$. This implies that the difference between N_s and N_o is the driving force of segregation into ODP. The larger the difference, the sharper the ODP becomes.

The area of the PD adjacent to $f_L = f_R = 1/2$ is occupied by *Stripy* ODPs. At small values of the filling fraction the phases are *Patchy*. A transition from *Stripes* to *Patches* occurs at $f_L \approx 0.38$ almost independently on parameter N_s/N_o. An example of such transition for $N_s/N_o = 3$ is shown in Figure 9.

The reasons for the transition for *small* values of $N_s/N_o - 1$ are discussed in Koulakov and Chklovskii, 1999. For *larger*differences, when ODP becomes sharp, the transition occurs due to the presence of surface contribution to the wire length. To demonstrate this we present the following argument, which is rigorously valid in the asymptotic limit of large number of connections to the same-eye neurons, i.e. $N_s >> N_o$. In this limit connections to the same-eye neurons are the most abundant and therefore most costly, from wire length prospective. Hence, we can disregard connections to the opposite-eye neurons in the first approximation. Consider a unit near the interface between two OD columns (top unit in Fig. 10). The connection arbor of this unit to the same OD units, shown by empty circles in Fig. 10, is strongly biased toward the home column, since the unit has to maintain certain number of connections there. This effect has been seen by Katz et al., 1989, in macaque striate cortex (see also the discussion in the Model Section above). For units away from the interface the connection arbor within the same OD column is close to a circle (Fig. 10 bottom unit). Thus, circular arbor renders the minimum wirelength in the absence of constraints, such as the interface between OD columns. With the interface present the connection arbor to the same eye neurons is therefore

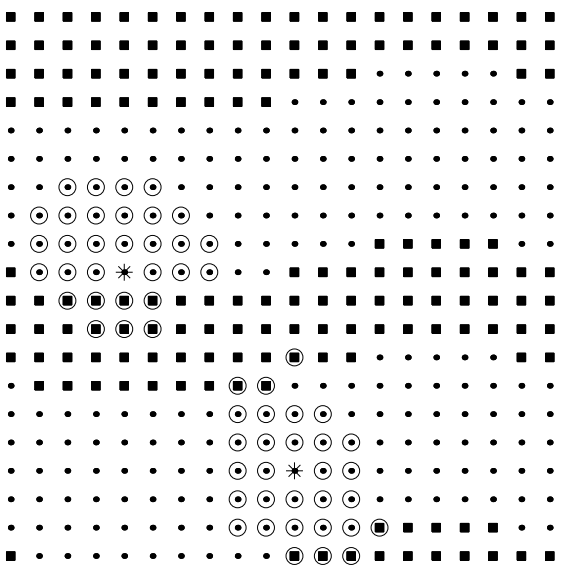

FIG. 10 Connection arbors of two units in the array: near the interface of OD columns (top) and in the center of a column (bottom). The units dominated by left and right eyes are shown by squares and dots respectively. Two units for which the arbors are displayed are shown by stars. They are connected to other units, which are encircled. The parameters for this particular layout are: $N_s = 23$, $N_o = 7$, $f_L = 0.40$. The connection arbor of the boundary unit (top) to the units of the same OD is significantly deformed, compared to the corresponding connection arbor of the unit in the middle of the column (bottom). This is similar to the observation of Katz et al., (1989). This deformation gives rise to the surface cost associated with formation of the interface between columns.

strongly deformed with respect to the optimum. Hence, the presence of the interface between the OD columns implies an increase in the wirelength, and is therefore associated with a surface cost (similar to Malsburg, 1979). This surface cost drives the transition from *Stripes* to *Patches*. Indeed if $f_L \ll 1/2$ the patchy phases have much shorter length of the surface compared to *Stripes*. This is because *Patches* shrink when $f_L \to 0$ reducing their surface length, whereas *Stripes* become narrower, keeping their surface length the same. However, this is not true for $f_L = f_R = 1/2$ where *Stripes* have a shorter surface for numerical reasons. Therefore, when f_L is decreased, the *Stripes* should unavoidably condense into *Patches* to minimize the surface cost. This is similar to droplets of water assuming circular shape to minimize the surface energy.

We conclude therefore that two important transitions occur in our model.

- The transition from unsegregated *Salt and Pepper* to weakly segregated and then sharp ODP is driven by the difference between parameters N_s and N_o characterizing the intra-cortical circuitry.
- The transition from *Stripy* to *Patchy* ODP is driven by the decreasing filling fraction of the ipsilateral eye and occurs at $f_L \approx 0.4$, if left eye is underrepresented.

C. Transition from *Stripes* to *Patches*: comparison to experiments

Our phase diagram in Fig. 8 shows that the transition from *Stripes* to *Patches* occurs when $f_L \approx 0.4$ for a wide range of N_s/N_o. This value will be compared now with the value of f_L at which the transition occurs in the experiment, found from the relative area occupied by left eye dominated neurons. The conclusion that the *Patch* phase becomes optimal when contralateral eye dominates is, indeed, non-trivial, because there may be a system of alternating wide and narrow monocular stripes instead.

We test our conclusion on the data from macaque monkey first (Horton and Hocking, 1996a). The relative area occupied by the left/right eye depends on the location in V1. In the parafoveal part of V1 both eyes are represented equally, i.e. $f_L \approx 0.5$. ODP has a stripy appearance, in agreement with the phase diagram. Away from the foveal region contralateral eye becomes dominant. The ODP becomes patchy there (LeVay et. al., 1985), just as expected from the theoretical phase diagram. We verify the location of the transition by using the following algorithm. We find f_L for each point of the pattern by calculating the relative area occupied by the left/right regions in a window centered on that point and a few OD periods wide (dashed lines in Fig. 11). Then we draw a contour corresponding to $f_L = 0.4$, Fig. 11. We observe in Fig. 11 that stripes indeed become patchy at the black contour indicating $f_R = 0.4$.

In *Cebus* monkey the ODP has a similar transition (Rosa et al., 1992). For monkey CO6L from Rosa et al., 1992, we determine visually that along the horizontal meridian the transition occurs at the eccentricity of $20 - 40$ deg. According to the plot of the relative representations given in Rosa et al., 1992, f_L changes in the range $0.32 - 0.42$ at these eccentricities. Our theoretical conclusion about a transition at $f_L = 0.4$ falls into this interval. For the upper 45 degree meridian of the same monkey the transition occurs at the eccentricity of $30-40$ degrees or at filling fractions $0.33 - 0.43$. Again, the predicted value belongs to this interval. We conclude that these data are consistent with the results of our model.

In cats the ODPs have a patchy appearance (Anderson et al., 1988; Jones et al., 1991). In this case our theory implies that one of the eyes should dominate. According to some reports (Shatz and Stryker, 1978; Crier et al., 1998) the filling fraction of the contralateral eye in cat V1 is about 0.8 in young animals (before P22). This may lead to *Patches* in cat V1. The strong contralateral bias disappears in older animals (Crier et al., 1998). This is consistent with other reports (Anderson et al., 1988) that both eyes are represented almost equally in adult cats.

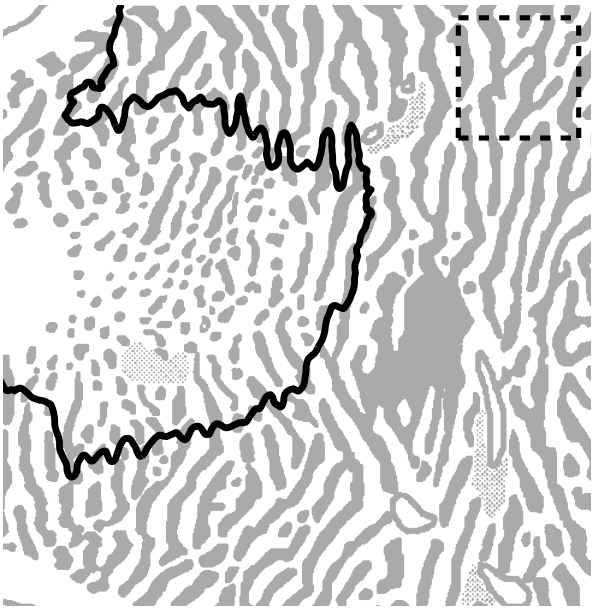

FIG. 11 Transition between the *Stripes* and *Patches* occurs at theoretically predicted value f_L. Shown is a fragment of the macaque ODP from Horton and Hocking (1996a). Areas dominated by the left eye are grey and neurons dominated by the left eye are white. The black contour corresponds to $f_L = 0.4$ averaged over a window, whose dimensions are shown by the dashed square (3.7×3.7mm). The points of transition from *Stripes* to *Patches* coincides with the black contour.

D. The period of ocular dominance pattern

1. Scalability of the Model

One of the general features of our model is that the period of OD pattern becomes larger, when the total number of connections is increased. Indeed, the size of the connection arbors grows if both N_s and N_o are increased, given that the density of units $(1/(30\mu \times 30\mu))$ is kept constant. This is because one has to go further to find the necessary number of connections to satisfy the wiring rules. Since dimensions of the connection arbors set up a characteristic scale for the OD pattern, the period of the latter also increases. This property of our model, which we call *scalability*, is discussed in this subsection.

Let us define scalability in a mathematically rigorous fashion. Assume that one has found a minimum wire length configuration for certain set of parameters N_s, N_o, and f_L (or $f_R = 1 - f_L$). Assume that both N_s and N_o are very large. In this case the dimensions of connection arbors are much larger than the lattice spacing, and one can ignore the fine structure imposed on the connection arbors by the square lattice. This is exactly the limit in which our model has some validity, both because realistic numbers of neuronal connections are large and because we would like to avoid artifacts introduced by the square lattice. An example of connection arbors for a neuron for some set of N_s and N_o are shown in Fig. 12 (left). This neuron and its connection arbors resemble the top neuron, marked by the star, in Fig. 10. The connection arbors in Fig. 12 look like continuous circular pieces, due to the large N_s and N_o limit (square lattice makes the boundaries of connection arbors look like staircases, whose steps are too small to show in the picture for large N_s and N_o). Imagine now a geometric transformation, in which the dimensions of the connection arbors of all of the neurons, as well as the OD pattern itself, are blown up by the same scaling factor $\eta > 1$. The two-dimensional density of the neurons must be preserved during this transformation. The obtained new OD pattern and the new connection arbors are shown schematically in Fig. 12 (right). Since the transformation is applied to the two-dimensional objects, and each of the dimensions was stretched by the factor η, each neurons in the new configuration will receive $\eta^2 N_s$ and $\eta^2 N_o$ connections from the same and opposite eye neurons. The newly obtained configuration (Fig. 12 right) will satisfy wiring rules with connection numbers given by $\eta^2 N_s$ and $\eta^2 N_o$. Note that the filling fraction is not changed by this transformation. It is $f_L = f_R = 1/2$ in Fig. 12. Will this be the minimum wire length configuration for this set of parameters?

To prove that the new configuration minimizes the total wire length for the new set of parameters $\eta^2 N_s$ and $\eta^2 N_o$ we notice that the total wirelength for the new configuration is given by $\eta^3 L$, where L is the total wirelength for the original configuration (Fig. 12 left). This is because each neuron now receives the number of connections increased by η^2, and each connection is stretched by η. Imagine now that one finds a new configuration, which has the total connection length $L' < \eta^3 L$. Let us take this more optimal configuration and shrink it by the factor of η. We obtain a configuration, satisfying wiring rules for the set N_s and N_o, whose total wirelength is $L'/\eta^3 < L$. But this contradicts to our postulate that the original configuration in Fig. 12 (left) is optimal for the set of parameters N_s and N_o. Thus the stretched configuration provides the minimum of the wirelength for the new set of parameters $\eta^2 N_s$ and $\eta^2 N_o$.

This property is important, because once the solution for given N_s and N_o is found, one can obtain other solutions, with the set of parameters $\eta^2 N_s$ and $\eta^2 N_o$, by stretching the original configuration by the factor of η uniformly in all the directions. The important property which remains the same for all these related configurations is the ratio between the numbers of the same and other eye connections, N_s/N_o. Thus, we conclude that this ratio determines the shapes of the OD patterns, which is unchanged during the uniform stretching procedure.

What is changed in the uniform stretching is the ODP period? Since the period is proportional to the stretching parameter η, while the total number of connections is proportional to η^2, we conclude that the period is proportional to the square root of the total number of con-

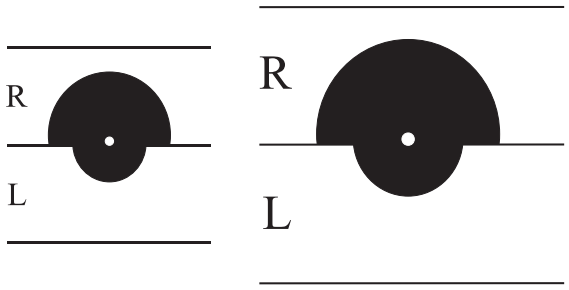

FIG. 12 The original ODP and connection arbor for one of the neurons, marked by the white dot (left). Compare to Fig. 10, top neuron. The stretched configuration is shown on the right.

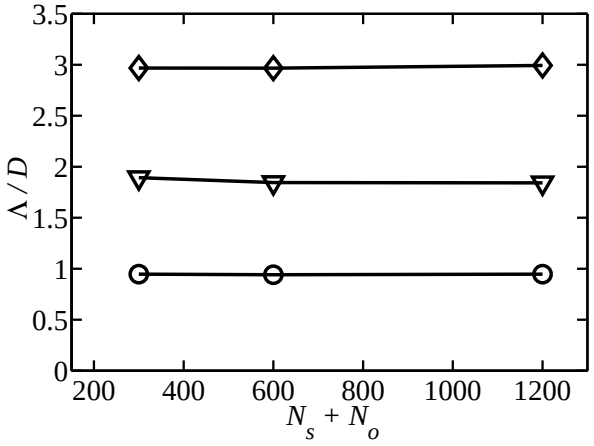

FIG. 13 The independence of the ratio Λ/D [see Eq.(5)] on the total number of connections. This implies that the lattice effects, violating scalability, are insignificant. The data are obtained for $f_L = 1/2$. Circles, triangles, and diamonds show results for N_s/N_o equal to 4/3, 17/3, and 14 respectively.

nections, when the ratio N_s/N_o is kept constant. This implies that

$$\Lambda\left(N_s, N_o, f_L\right) = D \cdot \lambda\left(N_s/N_o, f_L\right) \tag{5}$$

Here $D = 2a\sqrt{\left(N_s + N_o\right)/\pi} \sim \eta$, where $a = 30\mu$ is the size of the microcolumn unit. Parameter D has a meaning of the average axonal arbor diameter. The quantity $\lambda(N_s/N_o, f_L)$ is the *normalized OD period*, calculated in the units of the average axonal diameter. This quantity is introduced here for easier comparison to the experiment. Notice that this quantity does not depend on the total number of connections. The latter dependence is entirely absorbed by the parameter D.

Scalability is valid for the limit of large N_s and N_o, when square lattice effects can be ignored, and our model becomes continuous. Does scalability apply to our numerical solution, described in subsection II.B.3? To check this we plot the ratio $\Lambda\left(N_s, N_o, f_L\right)/D$, obtained using methods described in II.B.3, for different values of the total number of connections $N_s + N_o$ in Fig. 13. If Eq. (5) is valid, this ratio should not depend on the total number of connections. As evident from Fig. 13 this property is indeed satisfied. Hence, below in this subsection we always present the results for $\lambda\left(N_s/N_o, f_L\right) = \Lambda/D$, which are independent on the total number of connections, assuming that the latter dependence can be easily recovered using Eq. (5).

2. Dependence on parameter N_s/N_o

We now examine the dependence of normalized period $\lambda(N_s/N_o, f_L)$ [see Eq. (5)] on the parameter N_s/N_o, for $f_L = 1/2$, when we have to consider the stripe phase, according to subsection III.B. The results are shown in Fig. 14. These results have been obtained using methods described in subsection II.B.3. In general, the normalized period increases with increasing parameter N_s/N_o. This increase in the OD period can be understood considering the interplay between connections to the same and opposite eye units. Indeed, the presence of connections between the same eye units implies affinity between the same OD neurons. An increase in the relative number of such connections (N_s/N_o) strengthens such affinity. The OD columns provide a neighborhood rich with the same eye neurons; even more so, on average, for coarser domains. Thus stronger affinity between the same eye neurons (N_s/N_o) leads to an increase in the size of OD domains. This effect is produced by wiring economy principle, since the latter provides a substrate for the affinity of connected neurons.

We now examine Fig. 14 in more detail. The relative period diverges in the limit $N_s >> N_o$. The divergence can be described by the asymptotic formula

$$\lambda(N_s/N_o, f_L = 1/2) \approx 0.8\sqrt{\frac{N_s}{N_o}} \tag{6}$$

shown in Fig. 14 by the dotted curve. The divergence can be understood as follows. Imagine that the neurons do not have to connect to the neurons of the opposite OD, i.e. parameter $N_o = 0$, $N_s \neq 0$, which corresponds to the extreme case $N_s >> N_o$. In this case the optimum wire length configuration consists of only two large domains, dominated by left and right eye neurons, occupying a half of V1 each. This is because of the notion of surface contribution, introduced in subsection III.B. To minimize this interface contribution the system phase segregates into two large domains. Thus, in the case $N_o = 0$ ODP has maximum possible period, spanning the entire V1. This explains the tendency of the period diverge in the limit $N_o \neq 0$ $(N_s/N_o = \infty)$ in Fig. 14. What happens if $N_o \neq 0$? Since the neurons now have to connect to the opposite eye neurons, phase segregated configuration (two large domains spanning the entire V1)

is no longer optimum. The system introduces more interfaces between OD columns to shorten distances between opposite eye neurons. More interfaces implies a reduction in the OD period. Thus, finite N_s/N_o leads to the finite OD period. This is reflected by the asymptotic dependence (6) and the dotted curve in Fig. 14.

An interesting phenomenon observed in Fig. 14 is the presence of a few discontinuous changes in the OD period. One such a change occurs at $N_s/N_o \approx 1.15$ and consists in an abrupt increase in the OD period by a factor of about 2.3. Another discontinuous transition occurs at $N_s/N_o \approx 1.20$ and the corresponding increase in the period is by a factor of 2. Note that these transitions are truly discontinuous, i.e. they occur at discrete points. They appear smooth in Fig.14 due to a sparse sampling (the real data points are shown by dots). Note also that the quantity D in Eq. (5) changes negligibly in the interval between $N_s/N_o = 1.1$ and 1.2, which implies that both OD period Λ and the normalized period λ change approximately by the same factor. Such discontinuous changes in the OD period in the weakly segregated regime, i.e. when the ODP is not well defined, may be responsible for the coarsening of ODP in strabismic squirrel monkeys (see Discussion for more details).

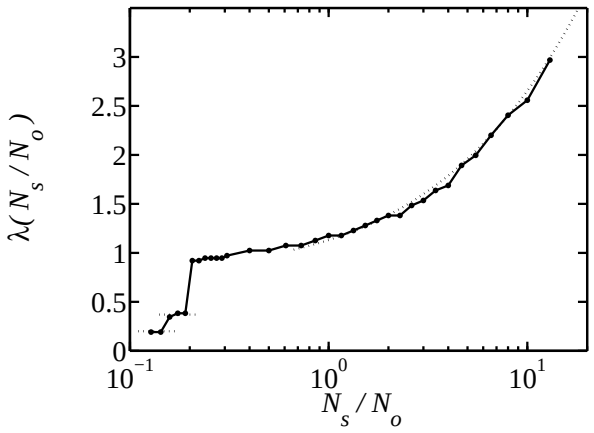

FIG. 14 Dependence of the normalized OD period, defined in Eq. (5), on the parameter N_s/N_o. The data points are shown by dots connected by lines. The dotted curve shows the asymptotic fit obtained for the values of parameters $N_s/N_o >> 1$ [Eq.(6)]. Two horizontal dotted lines show the plateau values of the period separated by discontinuous transitions at $N_s/N_o \approx 1.15$ and 1.20.

3. Dependence on the filling fraction

The dependence of the normalized period $\lambda(N_s/N_o, f_L)$ on the filling fraction of the left eye f_L is shown in Fig. 15. These results have been obtained using methods described in subsection II.B.3. Four dependencies are shown, for four values of the parameter N_s/N_o marked on each curve. The general tendency for the period to grow with increasing parameter N_s/N_o, described in the previous subsection, is evident in the Figure.

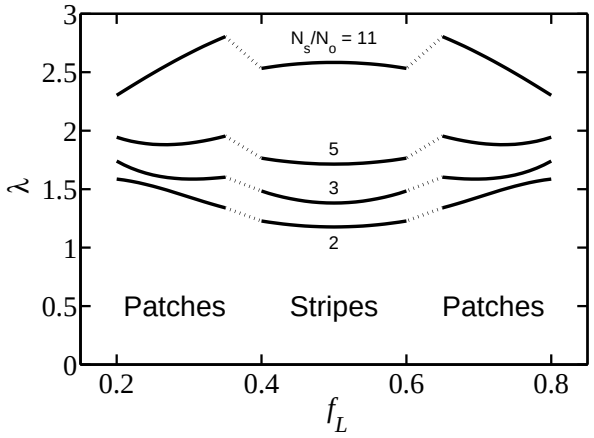

FIG. 15 The normalized OD period λ as a function of the filling fraction of one of the eyes. Four dependencies are shown for the values of parameter N_s/N_o equal to 2, 3, 5, and 11 correspondingly. The central segment of the dependencies, between $f_L = 0.4$ and 0.6 corresponds to the *Stripe* phase. The dependencies in the regions between $0.2 \le f_L \le 0.35$ and $0.65 \le f_L \le 0.8$ have been calculated for *Patches*, as indicated in the Figure. In the regions of transition between *Stripes* and *Pathes* the curves are connected by dotted lines.

For small values of parameter N_s/N_o the period increases when the filling fraction moves away from $f_L = 1/2$, as long as one stays within the same phase (*Stripes* or *Patches*). This behavior is seen for the two bottom curves in Fig. 15. In the transitional region between *Stripes* and *Patches* the OD period experiences a discontinuity, marked by the dotted lines. For large values of N_s/N_o, the dependence of the period on f_L is opposite: the period decreases, as the filling factor deviates from 1/2, as demonstrated by the top curve in Fig. 15.

We now compare this behavior of our model to the observations in the striate cortex of macaque monkey (Horton and Hocking, 1996a), using Fourier transform method described in subsection II.B.4. To make this comparison possible the following technical consideration is taken into account. The Fourier transform method evaluates the average value of the spatial frequency of the ODP $\langle Q \rangle$. The OD period is then calculated by the formula $\Lambda = 2\pi / \langle Q \rangle$. For the *Stripe* phase this procedure results in the value, which is close to the period of stripes. For *Patches* it results in the distance between rows of patches, which is smaller than the period by the factor $\sqrt{3}/2 \approx 0.87$ (see Fig. 16). Thus, to make comparison to the experiment possible, the values in Fig. 15 corresponding to *Patches* should be multiplied by the factor 0.87. The result of this procedure is shown in Fig. 17 by the gray line.

Fig. 17 shows that the period observed in the experiment decreases when the filling factor of the ipsilateral eye deviates from 1/2. This warrants the use of the top

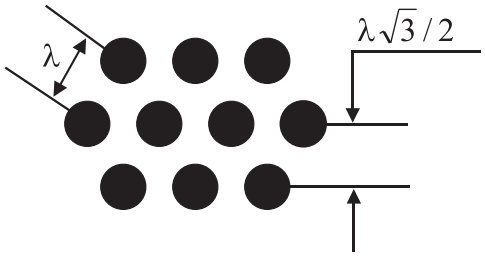

FIG. 16 For *Patches* Fourier transform produces distance between rows, rather then the period of the OD pattern. The distance between rows is a natural successor of the period of *Stripes* after the transition to *Patches* occurs (see also Fig. 9). The distinction between *Patch* period and distance between rows should be taken into account for accurate comparison to the experimental observations.

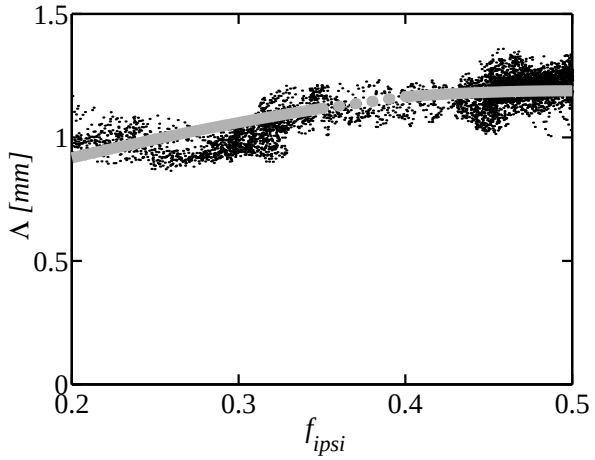

FIG. 17 Comparison of the OD period observed in the experiment (Horton and Hocking, 1996a) in macaque striate cortex (dots) to the results of our theory (gray curve). The former is obtained using Fourier transform method described in subsection II.B.4. The latter is the top curve in Fig. 15, with the sector of the data corresponding to *Patches* corrected by the factor $\sqrt{3}/2 \approx 0.87$ for compatibility with the Fourier transform. The only fitting parameter used is $D = 0.46$mm [see Eq. (5)].

curve in Fig. 15 to represent the theoretical result. Since, the shape of the theoretical dependence does not change much when $N_s/N_o > 10$, the parameter N_s/N_o cannot be established from the comparison of the theory to the experiment. To obtain the gray curve in Fig. 17 the $N_s/N_o = 11$ dependence in Fig. 15 was multiplied by the fitting parameter $D = 0.46$mm. This is the only fitting parameter used. As seen in Fig. 17, our theory describes the experimentally observed dependence quite well.

The widths of the ipsilateral and contralateral eye stripes in macaques has also been measured independently by Tychsen and Burkhalter (1997). Based on their results one can evaluate the ODP period and the filling fraction:

$$\Lambda = W_I + W_C, \quad f_{ipsi} = W_I/\left(W_I + W_C\right). \qquad (7)$$

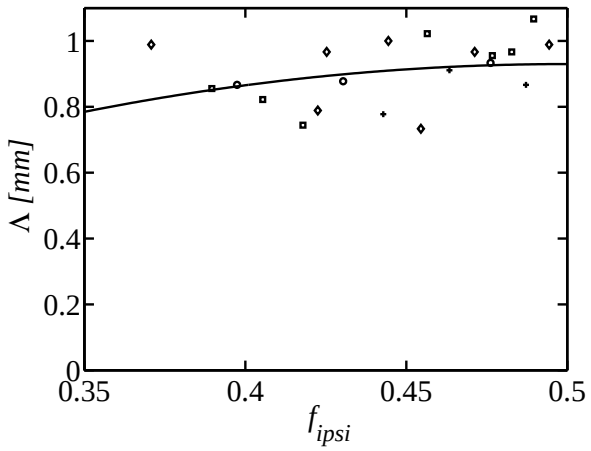

FIG. 18 The dependence of the ODP period on the filling fraction based on data from Tychsen and Burkhalter (1997). The results for non-strabismic adult macaque monkeys are presented by markers: monkeys M25 right V1 (diamonds), M25 left V1 (circles), 418 (squares), and 906 (dots). The curve shows the best parabolic fit (see text).

Here f_{ipsi}, W_I, and W_C are the filling fraction of the ipsilateral eye, and the ipsilateral/contralateral column widths respectively. The dependence of the period on the filling fraction can therefore be established. This dependence is shown in Fig.18.

The best parabolic fit to the data in Fig.18 is given by:

$$\Lambda(f) = \Lambda(1/2)\left[1 - \alpha\left(f_{ipsi} - 1/2\right)^2\right]. \qquad (8)$$

The coefficient $\alpha = -6.94 \pm 6.38$ is estimated using bootstrap (Efron and Tibshirani, 1993). The expectation value of the coefficient is therefore below zero, as seen from Fig.18. The probability of the coefficient to be greater than zero is $p = 0.11$ as evaluated by bootstrap procedure, which is used since the distribution of coefficients α is non-gaussian. This implies that with great degree of certainty one can assume that the period of ODP does decrease with the filling fraction deviating from 1/2.

It should be noted that the value of coefficient α can be obscured by the variability of ODP period between different individuals, since data in Fig.18 are assembled from three monkeys (four V1's). To reduce the impact of inter-individual variability we then normalized the period for each area V1 by the mean value for each individual animal. The value of the coefficient is then $\alpha = -7.98 \pm 6.24$, with the probability of positive coefficient $p = 0.055$. Thus the decrease of the period with filling fraction is even more certain, when the inter-individual variability is accounted for. The value of coefficient α obtained from the theory is 2 (Fig. 15, $N_s/N_o = 11$). It is consistent with both measurements.

IV. DISCUSSION

In this work we propose a model which can account for most of experimentally observed features of ODPs. Our model has two principal parameters. The first parameter characterizes the intracortical circuitry. It is the difference between the number of connections to the same and to the opposite OD neurons. Our results suggest that this difference is the driving force of segregation into ODPs. We argue therefore that the sensitivity of the intra-cortical connectivity to OD provides a reason to formation of OD columns (see below). The second parameter is the fraction of neurons dominated by the ipsilateral eye. This parameter determines the shape of monocular regions in ODP. In the majority of the primary visual area of macaque and *Cebus* monkeys this parameter is close to 50%, which implies that both ipsi- and contralateral eyes are equally represented. However, in the proximity of monocular crescent the ipsilateral eye becomes underrepresented. This is because the inputs into the eye are blocked by the nose of the animal. Our theory suggests that the decrease in the filling fraction of the ipsilateral eye drives the transition in the ODP structure from stripy (zebra skin like) to patchy (similar to leopard skin). The transition occurs when the fraction of the ipsilateral eye dominated neurons approaches 40% in both macaque and *Cebus* monkeys (see below). We also analyze the dependence of OD period on the parameters of our model and find satisfactory agreement with experimental data.

A. On the functional significance of OD columns

Each neuron in our model establishes certain number of intra-cortical connections with neurons dominated by the same and the opposite eye. As suggested by experimental studies in macaque striate cortex, neurons in layer $4C\beta$ typically make more connections with neurons of the same OD (Katz et al., 1989). Thus, from wiring economy prospective, connections with neurons of the same OD are more important than the opposite eye connections. Therefore, it is advantageous to form OD columns, since they provide environment rich with the same OD neurons, which results in shortening connections to the same eye neurons. The wiring economy principle thus provides a natural reason for the existence of OD patterns, i.e. answers the first question in the program listed in the Introduction.

Our model suggests that in primates with weakly defined OD columns, such as squirrel monkey (Hubel et al., 1976; Livingstone, 1996; Horton and Hocking, 1996b) and owl monkey (Livingstone, 1996), the difference between these two components of intracortical connectivity is not large. Such difference may be increased in these animals by experimentally induced strabismus. Indeed, strabismus reduces correlated activity between opposite OD cortical neurons, therefore reducing their connectivity N_o. Reduction in N_o unbalanced by the corresponding reduction in N_s increases the parameter N_s/N_o and leads to sharpening of OD columns, according to our phase diagram in Fig. 8. Such sharpening is indeed observed experimentally (Shatz et al., 1977; Lowel, 1994; Livingstone, 1996). This phenomenon was also predicted theoretically by Goodhill (1993).

The two parameters of intra-cortical circuitry, N_s and N_o, represent in our model the interplay between two classes of processing performed by the visual cortex. The first class includes the processing of the monocular image, for which connections to the same OD neurons are necessary. The second class includes various tasks related to stereopsis, which require comparison of two monocular images, relying on the connections between the opposite OD neurons. We proposed above that the function of OD columns is to shorten the connections between the same eye neurons. The impact of stereoscopic vision should therefore be the opposite: strong stereoscopy should make ODP weaker. Inversely, weak stereoscopy induces sharp ODPs. The latter statement is justified by the observations in animals with experimental strabismus. However, one should be careful about this statement, since the relation between functional and anatomical properties may not be direct.

The situation in the animals with lateral eye positioning, such as mice, rats, tree shrews, etc., is different. In such animals the visual pathway is almost completely crossed, i.e. V1 in each hemisphere is strongly dominated by the contralateral eye [Drager, 1974, 1975, 1978; Drager and Olsen, 1980; Gordon and Stryker, 1996 (mouse); Hubel, 1977 (rat); Casagrande and Harting, 1975; Mully and Fitzpatrick, 1992 (tree shrew); Horton and Hocking, 1996b (other species)]. As suggested by Antonini et al. (1999) this implies that the ODP contains only two large monocular 'columns', each spanning the whole hemisphere. This can be interpreted as an OD having very large period, spanning both striate cortices. This picture can be fitted into the framework of our model. Indeed, we predict that if the number of connections to the other OD neurons (N_o) is very small the OD has a very large period (Fig.14). Thus our model predicts that the number of connections received by each neuron from the neurons of the same OD (N_s) is much larger than the number of opposite eye connections (N_o) in the species with lateral eye positioning. This should include the cross-hemispheric projections. This statement should have functional consequences. Since N_o is small, synthesis of images from two eyes is weaker. Therefore the animals have to find another strategy to implement stereopsis. Hooded rats for example use vertical head movements to estimate distances (Legg and Lambert, 1990). Our conclusion about small N_o should also apply to the superior colliculus in these animals (Colonnese and Constantine-Paton, 2001), as well as to the tectum in lower vertebrates (Schmidt and Tieman, 1985), in which cases the visual inputs cross over almost completely too.

To summarize, our model encompasses most of the

phenomena related to the sharpness and observability of ODP. It relates the interspecies variability in the ODP to the relative amount of binocular interaction occurring in different species. Thus, we predict, that in the animals with weakly segregated columns (squirrel monkey) $N_s \approx N_o$; in the animals with sharp columns (macaque) N_s is much larger than N_o [confirmed by Katz et al., (1989)]; and, finally, in the animals with lateral eye positioning, N_o should have a value, whose contribution to the wirelength can be neglected.

B. Variation of the ODP period in the extrafoveal region

Another consequence of a decreasing f_L in macaque is a decrease in the ODP period (LeVay et al., 1985). In Fig. 17 we compare the result of our theory to the data from macaque monkey (Fourier transform applied to data from Horton and Hocking, 1996a). From this comparison we conclude that, according to the wiring economy principle, parameter $N_s/N_o >> 1$, or cells establish much more connection with the same OD cells, than with the opposite. This result of is consistent with the observations of OD sensitive circuitry in the striate cortex of macaque by Katz et al. (1989).

We chose the regions proximal to the horizontal meridian for this comparison. This is based on the assumption that cortical properties, such as N_s and N_o, change little along this meridian. This assumption is in part supported by the fact that OD periodicity changes little on the large segment of the meridian occupied by stripes, spanning the region between about 2 and 25 degree eccentricity (notice very little scatter in Fig. 17 around the point $f_L = 1/2$). The changes in the period begin to occur when f_L deviates from 1/2. This is illustrated by Fig. 17. Other authors notice a decrease in the period when comparing vertical to horizontal meridian. Studies based of computer reconstructions report about 2 fold decrease in OD periodicity comparing these areas (LeVay et. al., 1985), while others, based of flat-mounts (Horton and Hocking, 1996a), report a more moderate change. Such variation cannot be accounted for by a decrease in parameter f_L alone, since f_L is about 1/2 on both meridians in close proximity to parafoveal region (¡20 degrees of eccentricity). Our model suggests two possibilities based on the variation in the intracortical circuitry, described by N_s and N_o. Since such differences in the circuitry may also be responsible for variability of the OD period between different animals, we discuss this possibility in the next subsection.

C. Variability of the ODP period from individual to individual

Studies in macaque monkeys (Horton and Hocking, 1996a) reveal large inter-individual variability of the stripe period. The stripe period is $1072 \pm 164\mu$ along the V1 border, after comparison of 6 animals. Two factors may contribute to this phenomenon in the framework of our model. (1) The basic diameter of axonal and dendritic arbors D varies from animal to animal. This could be due to changes in N_s, N_o, or neuronal density. (2) The ratio between monocular and binocular interactions N_s/N_o varies. The former reason is justified by Eq. (5). The latter can be understood from Fig. 14. Simply speaking, monocular interactions (N_s) favor formation of OD columns, making them wider, in an effort to provide same OD rich environment for all the neurons. Binocular interactions (N_o) favor interfaces between columns, since interfaces bring opposite OD neurons closer to each other. They therefore decrease OD period. When N_s/N_o increases the OD period increases too (Fig. 14). This may occur when comparing different individuals.

D. ODP period in strabismic animals

Similar consideration may apply to the experiments in strabismic animals (Lowel, 1994; Livingstone, 1996). Since strabismus reduces correlations between eyes, its effect in our model is to reduce parameter N_o. Hence, the ratio N_s/N_o is increased. According to our model (Fig. 14) this generally leads to an increase in the relative OD period (ratio of the basic OD periodicity to the connection range D). This result is understood from the interplay between affinity between the same eye neurons (N_s), increasing the period, and the affinity between opposite OD neurons (N_o), reducing OD period. Since the latter is reduced by strabismus, the OD period grows.

The degree of the period change depends on the decrease in the number of interocular connection, and is difficult to estimate. A curious feature displayed by OD period in our model is an abrupt increase at $N_s/N_o \approx 1.15$ by a factor of about 2.3, cf. Fig. 14. This implies that close to point $N_s/N_o = 1.15$ the OD period may be very sensitive to developmental manipulations. This finding may have correlate in squirrel monkey, for which the observed increase in period is by a factor $2.9 - 3.6$ (Horton and Hocking, 1996b). These data are obtained from comparison to a single strabismic animal. The following scenario is possible, comparing squirrel monkey to the strabismus experiments in owl monkey (Livingstone, 1996), in which no significant increase in periodicity is observed. Parameter N_s/N_o in squirrel monkey passes the point $N_s/N_o = 1.15$ due to strabismus, leading to the substantial increase in period. In owl monkey parameter N_s/N_o is above 1.15 in normal animal. Strabismus therefore has little effect. This scenario is consistent with sharper OD columns in normal owl monkeys ($N_s/N_o > 1.15$) than in normal squirrel monkeys ($N_s/N_o < 1.15$) (Livingstone, 1996; Horton and Hocking, 1996b). Experimentally induced strabismus in cat leads to an increase in the OD period by a factor of 1.3 (Lowel, 1994; Goodhill, 1993; see however Jones et al., 1996). Our model suggests that parameter $N_s/N_o > 1.15$ in cat, and the increase in the period is due to the smooth part of the dependence in

Fig. 14, which may not be so substantial as in squirrel monkey.

E. On the importance of wiring minimization

The relevance of wiring economy principle to the neuronal spatial organization can be illustrated by the following thought experiment (Koulakov and Chklovskii, 2001). Imagine taking a cortical area and scrambling neurons in that area, while keeping all the connections between neurons the same. Since the circuit is unchanged, the functional properties of the neurons remain intact. Therefore, from the functional point of view, the scrambled region is identical to the original one. In fact, the only difference caused by scrambling is in the length of neuronal connections. Therefore, it is hard (if not impossible) to justify the existence of systematic cortical maps, such as OD pattern, without invoking the cost of making long neuronal connections. Although some theories of map formation may not explicitly mention the wiring optimization principle, it is present implicitly, usually in requiring the locality of intra-cortical connections.

How important is the constraint imposed by wiring minimization? In principle one can imagine development of an organism, which has 30% excess of wire with respect to the existing ones. It turns out that the existence of such an organism is close to impossible. Indeed, imagine that an external object, such as a blood vessel, is introduced in certain area of the gray matter. In this case some of the neuronal connection have to go around the vessel, therefore increasing in length. If the nerve pulses are to be delivered at the original speed and/or intensity, the elongated axons and dendrites have to be made thicker, to increase the pulse propagation speed and decrease dendritic attenuation. This leads to more obstacles on the way of other neuronal connections and so on. Thus, introduction of a new blood vessel leads to an infinite series of axonal and dendritic reconstructions. The same is true about the extra connection volume, resulting from wasteful neuronal positioning. Such infinite series of reconstructions can diverge, which implies that the connection volume resulting from more and more reconstructions increases indefinitely. In this case the new blood vessel can never be inserted without sacrificing significantly the brain function. It turns out that mammalian brain has reached the verge of this so called *wiring catastrophe* (Chklovskii and Stevens, 2001), so that it gets increasingly more difficult to accommodate excess volume in the nerve tissues.

The wiring catastrophe occurs when the fraction of axons and dendrites in the cortical volume reaches 60%. Electron microscopy studies of cortical slices show that the actual volume occupied by neuronal processes is about 55% (Chklovskii and Stevens, 2001). The brain therefore has approached the barrier imposed by wiring catastrophe. Further increase of the volume fraction of neuronal processed may deteriorate the brain function.

F. Comparison to other models

As discussed in the previous subsection, wiring optimization is the only known way to relate neuronal layout (as manifested in the ODP) to the statistics of neuronal connectivity. Models of the ODP development that do not explicitly rely on wiring optimization invoke it implicitly, usually requiring the locality of intra-cortical connections.

Here we discuss the relationship of our model to the models that invoke wiring optimization explicitly.

In his pioneering work, Mitchison (1991) studied a question whether ODP minimize the wiring volume relative to the *Salt and Pepper* layout. He assumed that the inter- neuronal connectivity is determined both by ocular dominance and retinotopy with all neurons having the same connectivity rules. He found that the answer to this question depends on the detailed assumptions about axonal branching rules. In particular it depends on the value of axonal branching exponent α. He has shown that if all axonal segments have the same caliber ($\alpha = \infty$), than ODP's are indeed advantageous for certain range of ratios of same-eye to opposite-eye connections. He also showed that if $\alpha < 4$ than the ODP do not save wiring volume relative to *Salt and Pepper*. However, existing data seems to suggest that axonal caliber branches with $\alpha < 4$ (Deschenes and Landry 1980, Adal and Barker, 1965).

The case of axonal branching with the cross-sectional area conservation corresponds closely to our model because we require a separate connection for each neuron. The reason we find that ODP minimize wiring length is because we drop the retinotopy requirement on interneuronal connection rules, an assumption supported by the experimental data (Katz). Although, effectively connections are roughly retinotopic, connection rules may vary from neuron to neuron thus providing some flexibility. The advantage of our approach is its simplicity allowing us to map out a complete phase diagram and make experimentally testable predictions. The full theory of the ODP will require a detailed analysis of axonal branching which must rely on better knowledge of axonal branching rules.

Jones et al. (1991) proposed an explanation for why ODP have either Stripy or Patchy appearance. They assumed that neurons are already segregated into the ODP (by considering units whose size equals the width of monocular regions) and found that the difference between Stripy and Patchy appearances of the ODP could be due to the boundary conditions, i.e. different shape of V1 in different species. Although the correlation between the shape of V1 and the ODP layout is observed, the model of Jones et al. does not explain why peripheral representation of macaque V1 has patchy ODP or why ocular dominance stripes run perpendicular to the long axis of V1 in some parts of V1 but not in others. Moreover, it is the local structure of ODP that is likely to determine the shape of V1 and not the other way around. Therefore,

unlike Jones et al., our work proposes a unified theory of ODP including *Salt and Pepper*, Stripy and Patchy layouts, and is based on local inter-neuronal connectivity rules.

Another model related to wiring length minimization is the elastic net model studied by Goodhill and coworkers (1993). The original formulation of the model minimized the cost function which penalized for placing nearby neurons whose activity is not correlated, a choice justified by computational convenience. Later the elastic model was generalized by the introduction of a C measure. Maximization of C measure effectively corresponds to penalizing for placing correlated neurons far apart. Unlike wiring optimization the penalty does not increase beyond a distance called cortical interaction. Because of this, elastic net often yields solutions where left and right eye neurons are completely segregated into left and right eye maps.

Our wiring optimization models can be viewed as a sub-set of models described by C measure. The advantage of our wiring optimization approach is that it has a transparent biological justification for the cost of placing neurons far from each other - the cost of wiring. Because of this, wiring optimization is a natural choice for questions related to the anatomy of intra-cortical connections.

Wiring optimization provides a link between neuronal connectivity and spatial layout. Thus, it leaves open the connection between connectivity and computational function. Unlike most other models, which assume that neurons should be connected only if they are correlated, wiring optimization makes other assumptions about connectivity possible, for example connecting neurons with anti-correlated firing.

G. Conclusion

Our theory relates functional requirements on the neuronal circuits to its structural properties. In particular, our model relates the amounts of the neuronal intraocular and interocular interactions, and the filling fraction of ipsilateral neurons, to the structure of the ocular dominance pattern. We conclude that the interspecies variability in the ocular dominance patterns may be explained by differences in the underlying cortical circuitry.

References

[1] Adal MN, Barker D (1965) Intramuscular branching of fusimotor fibers. J Physiol 177:288-299.

[2] Ahmed B, Anderson JC, Douglas RJ, Martin KA, Nelson JC (1994) Polyneuronal innervation of spiny stellate neurons in cat visual cortex. J Comp Neurol 341:39-49.

[3] Allman JM, Kaas JH (1974) The organization of the second visual area (V II) in the owl monkey: a second order transformation of the visual hemifield. Brain Res 76:247-265.

[4] Anderson PA, Olavarria J, Van Sluyters RC (1988) The overall pattern of ocular dominance bands in cat visual cortex. J Neurosci 8:2183-2200.

[5] Antonini A, Fagiolini M, Stryker MP (1999) Anatomical correlates of functional plasticity in mouse visual cortex. J Neurosci 19:4388-4406.

[6] Blasdel GG, Fitzpatrick D (1984) Physiological organization of layer 4 in macaque striate cortex. J Neurosci 4:880-895.

[7] Cajal SRy (1995) Histology of the nervous system of man and vertebrates. New York: Oxford University Press.

[8] Casagrande VA, Harting JK (1975) Transneuronal transport of tritiated fucose and proline in the visual pathways of tree shrew Tupaia glis. Brain Res 96:367-372.

[9] Cherniak C (1992) Local optimization of neuron arbors. Biol Cybern 66:503-510.

[10] Chklovskii DB, Koulakov AA (2000) A wire length minimization approach to ocular dominance patterns in mammalian visual cortex. Physica A 284:318-334.

[11] Chklovskii DB (2000) Binocular disparity can explain the orientation of ocular dominance stripes in primate primary visual area (V1). Vision Res 40:1765-1773.

[12] Colonnese MT, Constantine-Paton M (2001) Chronic NMDA receptor blockade from birth increases the sprouting capacity. J Neurosci 21:1557-1568.

[13] Cowey A (1979) Cortical maps and visual perception: the Grindley Memorial Lecture. Q J Exp Psychol 31:1-17.

[14] Crair MC, Gillespie DC, Stryker MP (1998) The role of visual experience in the development of columns in cat visual cortex. Science 279:566-570.

[15] Deschenes M, Landry P (1980) Axonal branch diameter and spacing of nodes in the terminal arborization of identified thalamic and cortical neurons. Brain Res 191:538-544.

[16] Drager UC (1974) Autoradiography of tritiated proline and fucose transported transneuronally from the eye to the visual cortex in pigmented and albino mice. Brain Res 82:284-292.

[17] Drager UC (1975) Receptive fields of single cells and topography in mouse visual cortex. J Comp Neurol 160:269-290.

[18] Drager UC (1978) Observations on monocular deprivation in mice. J Neurophysiol 41:28-42.

[19] Drager UC, Olsen JF (1980) Origins of crossed and uncrossed retinal projections in pigmented and albino mice. J Comp Neurol 191:383-412.

[20] Efron B, Tibshirani R (1993) An introduction to the bootstrap. New York: Chapman and Hall.

[21] Erwin E, Obermayer K, Schulten K (1995) Models of orientation and ocular dominance columns in the visual cortex: a. Neural Comput 7:425-468.

[22] Goodhill GJ (1993) Topography and ocular dominance: a model exploring positive correlations. Biol Cybern 69:109-118.

[23] Gordon JA, Stryker MP (1996) Experience-dependent plasticity of binocular responses in the primary visual cortex of the mouse. J Neurosci 16:3274-3286.

[24] Horton JC, Hocking DR (1996) Intrinsic variability of ocular dominance column periodicity in normal macaque monkeys. J Neurosci 16:7228-7239.

[25] Horton JC, Hocking DR (1996) Anatomical demonstration of ocular dominance columns in striate cortex of the squirrel monkey. J Neurosci 16:5510-5522.

[26] Hubel DH, Wiesel TN (1965) Binocular interaction in

striate cortex of kittens reared with artificial squint. J Neurophysiol 28:1041-1059.

[27] Hubel DH, Wiesel TN (1969) Visual area of the lateral suprasylvian gyrus (Clare-Bishop area) of the cat. J Physiol 202:251-260.

[28] Hubel DH, Wiesel TN (1974) Uniformity of monkey striate cortex: a parallel relationship between field size, scatter, and magnification factor. J Comp Neurol 158:295-305.

[29] Hubel DH, Wiesel TN (1977) Ferrier lecture. Functional architecture of macaque monkey visual cortex. Proc R Soc Lond B Biol Sci 198:1-59.

[30] Jones DG, Van Sluyters RC, Murphy KM (1991) A computational model for the overall pattern of ocular dominance. J Neurosci 11:3794-3808.

[31] Jones DG, Murphy KM, Van Sluyters RC (1996) Spacing of ocular dominance columns is not changed by monocular deprivation or strabismus. Invest Ophtalmol Vis Sci 37:1964.

[32] Katz LC, Gilbert CD, Wiesel TN (1989) Local circuits and ocular dominance columns in monkey striate cortex. J Neurosci 9:1389-1399.

[33] Koulakov AA, Chklovskii DB (2001) Orientation preference patterns in mammalian visual cortex: a wire length minimization approach. Neuron 29:519-527.

[34] LeVay S, Gilbert CD (1976) Laminar patterns of geniculocortical projection in the cat. Brain Res 113:1-19.

[35] LeVay S, Connolly M, Houde J, Van Essen DC (1985) The complete pattern of ocular dominance stripes in the striate cortex and visual field of the macaque monkey. J Neurosci 5:486-501.

[36] Livingstone MS (1996) Ocular dominance columns in New World monkeys. J Neurosci 16:2086-2096.

[37] Lowel S (1994) Ocular dominance column development: strabismus changes the spacing of adjacent columns in cat visual cortex. J Neurosci 14:7451-7468.

[38] Mitchison G (1991) Neuronal branching patterns and the economy of cortical wiring. Proc R Soc Lond B Biol Sci 245:151-158.

[39] Mountcastle VB (1957) J Neurophysiol 20:408-434.

[40] Muly EC, Fitzpatrick D (1992) The morphological basis for binocular and ON/OFF convergence in tree shrew striate cortex. J Neurosci 12:1319-1334.

[41] Peters A, Payne BR, Budd J (1994) A numerical analysis of the geniculocortical input to striate cortex in the monkey. Cereb Cortex 4:215-229.

[42] Rockel AJ, Hiorns RW, Powell TP (1980) The basic uniformity in structure of the neocortex. Brain 103:221-244.

[43] Rosa MG, Gattass R, Fiorani M, Jr., Soares JG (1992) Laminar, columnar and topographic aspects of ocular dominance in the primary visual cortex of Cebus monkeys. Exp Brain Res 88:249-264.

[44] Schmidt JT, Tieman SB (1985) Eye-specific segregation of optic afferents in mammals, fish, and frogs: the role of activity. Cell Mol Neurobiol 5:5-34.

[45] Shatz CJ, Lindstrom S, Wiesel TN (1977) The distribution of afferents representing the right and left eyes in the cat's visual cortex. J Neurosci 16:5510-22.

[46] Shatz CJ, Stryker MP (1978) Ocular dominance in layer IV of the cat's visual cortex and the effects of monocular deprivation. J Physiol 281:267-283.

[47] Swindale NV (1980) A model for the formation of ocular dominance stripes. Proc R Soc Lond B Biol Sci 208:243-264.

[48] Swindale NV (1996) The development of topography in the visual cortex: a review of models. Network: Computation in Neural Systems 7:161-247.

[49] Tychsen L, Burkhalter A (1997) Nasotemporal asymmetries in V1: ocular dominance columns of infant, adult, and strabismic macaque monkeys. J Comp Neurol 388:32-46.

[50] von der Malsburg C (1979) Development of ocularity domains and growth behaviour of axon terminals. Biol Cybern 32:49-62.

[51] Wiesel TN, Hubel DH, Lam DM (1974) Autoradiographic demonstration of ocular-dominance columns in the monkey striate cortex by means of transneuronal transport. Brain Res 79:273-279.

[52] Young MP (1992) Objective analysis of the topological organization of the primate cortical visual system. Nature 358:152-155.